Supporting Information

Self-Sensing Coaxial Muscle Fibers with Bi-Lengthwise Actuation

Lizhong Dong,[ab] Ming Ren,[ab] Yulian Wang,[ab] Jian Qiao,[b] Yulong Wu,[b] Jianfeng He,[ab] Xulin Wei,[ab] Jiangtao Di*[abc] and Qingwen Li*[abc]

[a.] School of Nano-Technology and Nano-Bionics, University of Science and Technology of China, Hefei 230026, China

[b.] Advanced Materials Division, Key Laboratory of Multifunctional Nanomaterials and Smart Systems, Suzhou Institute of Nano-Tech and Nano-Bionics, Chinese Academy of Sciences, Suzhou 215123, China

[c.] Division of Nanomaterials, Suzhou Institute of Nano-Tech and Nano-Bionics, Chinese Academy of Sciences, Nanchang 330200, China

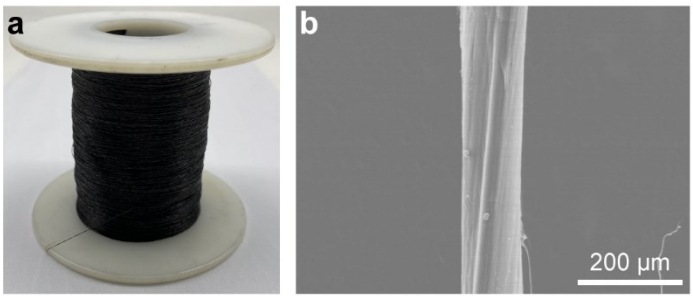

Fig. S1 (a) Photograph of a hundreds-meter-long CNT fiber winded on a mandrel. (b) SEM image of the surface of the CNT fiber. The diameter of the CNT ribbon is ~122 μm.

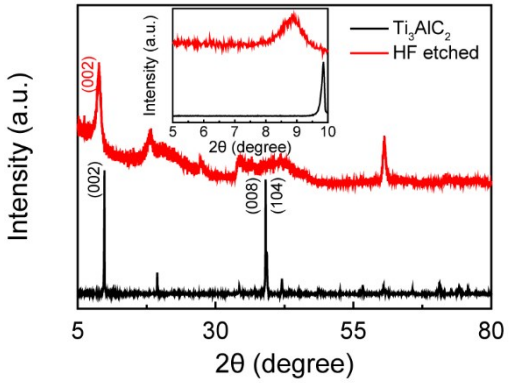

Fig. S2 XRD patterns of Ti_3AlC_2 MAX phase and $Ti_3C_2T_x$.

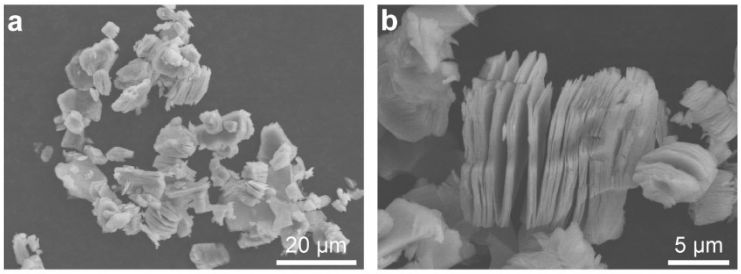

Fig. S3 SEM images of $Ti_3C_2T_x$.

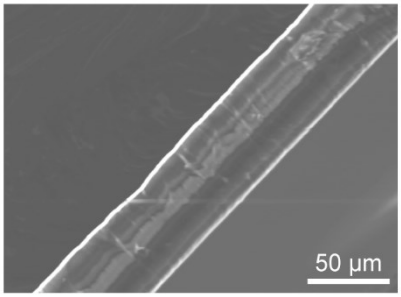

Fig. S4 The thickness of the PDMS ribbon (50 μm).

Fig. S5 Photograph of the PDMS ribbon, the width is 5 mm.

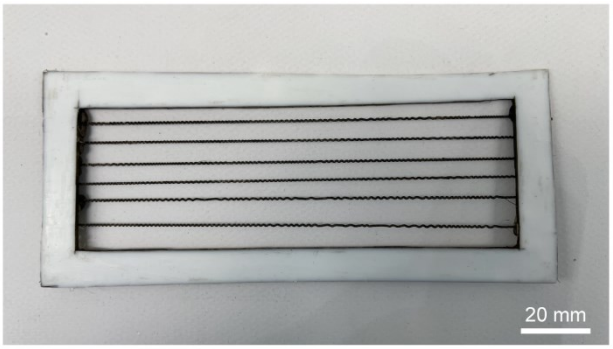

Fig. S6 Photograph of the pre-stretched CNT@PDMS coaxial fiber polymerized by dopamine (polymerized for 48 h at 30 °C).

Fig. S7 Photograph of the MXene and SWCNTs 3D conductive network dispersion.

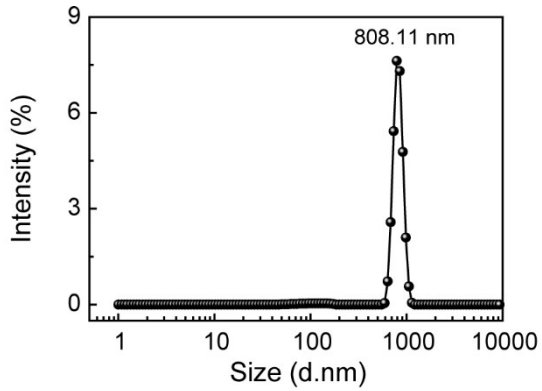

Fig. S8 Average particle size distribution of $Ti_3C_2T_x$.

Fig. S9 Water contact angle corresponding to different fibers. (a) The CNT@PDMS coiled coaxial fiber. (b) The CNT@PDMS coiled coaxial fiber after oxygen plasma treatment. (c) The CNT@PDMS coiled coaxial fiber after polymerizing dopamine. (d) The MXene/SWCNTs-coated CNT@PDMS coiled coaxial fiber.

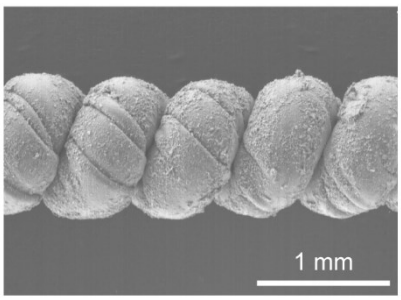

Fig. S10 The SEM image of the MXene/SWCNTs-coated CNT@PDMS coaxial muscle fiber.

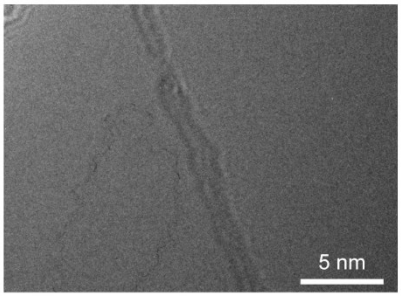

Fig. S11 TEM image of the typical SWCNTs in the MXene and SWCNTs 3D conductive network, showing the CNTs have one graphitic wall and the diameter is ~1-3 nm.

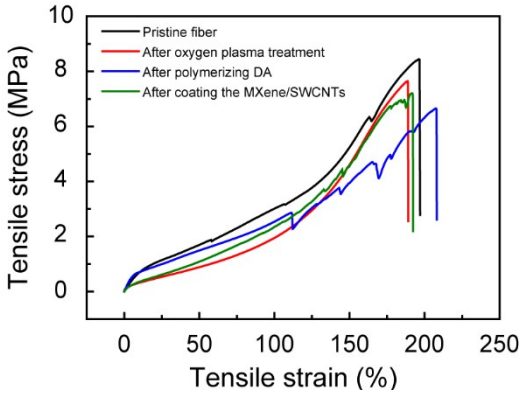

Fig. S12 Mechanical properties corresponding to different fibers (the CNT@PDMS coiled coaxial fiber, the CNT@PDMS coiled coaxial fiber after oxygen plasma treatment, the CNT@PDMS coiled coaxial fiber after polymerizing dopamine, the MXene/SWCNTs-coated CNT@PDMS coiled coaxial fiber).

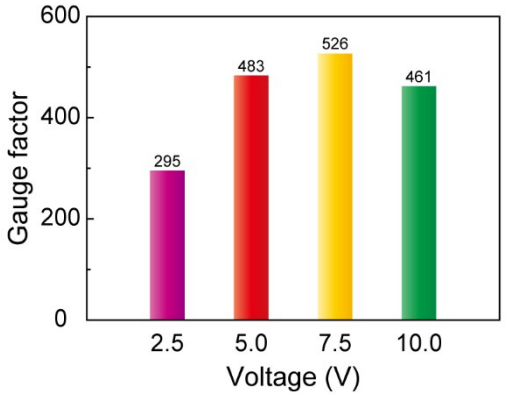

Fig. S13 The gauge factor of real-time sensing feedback signal during contractile process under different voltages.

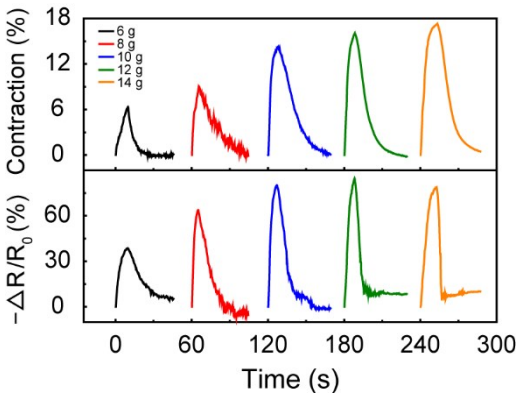

Fig. S14 Contraction and relative resistance change ($-\Delta R/R_0$) as a function of time under a 10 V voltage with different loads.

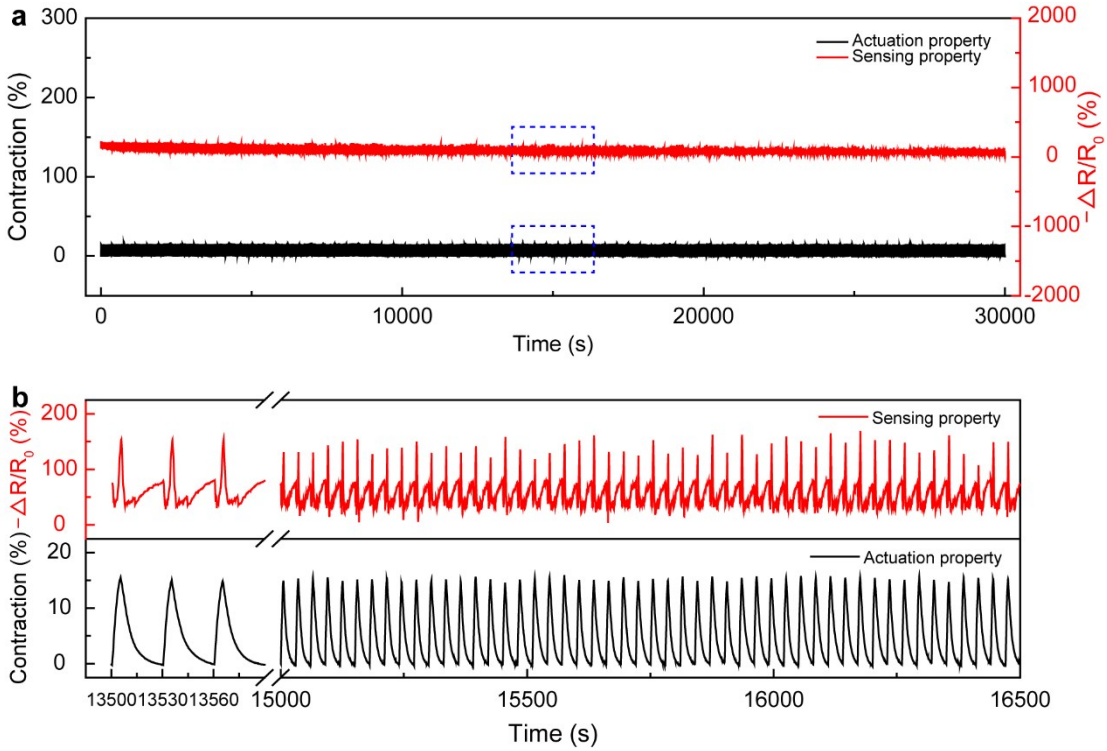

Fig. S15 (a) Cyclic tests of the contraction with real-time sensing signal feedbacks (under a 10 V voltage with a 14 g load, powering on for 5 s and powering off for 25 s) on the MXene/SWCNTs-coated CNT@PDMS coaxial muscle fiber, 1 000 actuating cycles. (b) The curve of the 100 actuating cycles with real-time sensing signal feedbacks from 450th to 550th.

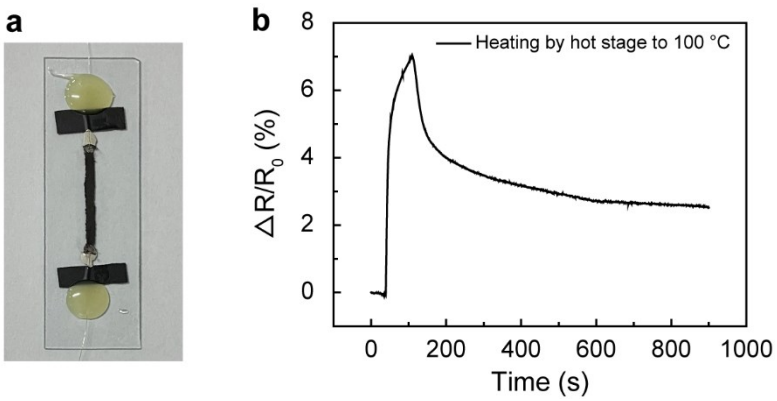

Fig. S16 (a) Photograph of a device for measuring sensing signal on the hot stage of the MXene/SWCNTs 3D conductive network sensing layer. (b) The sensing signal of the MXene/SWCNTs 3D conductive network sensing layer was measured by a 100 °C hot stage.

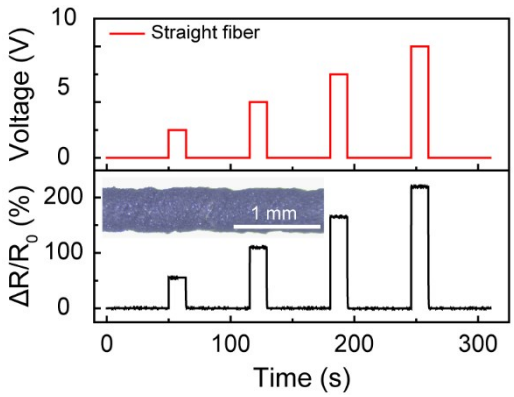

Fig. S17 The sensing property of the MXene/SWCNTs-coated CNT@PDMS straight coaxial fiber with restricted length under different voltage. The inset is the photograph under the optical microscope of the MXene/SWCNTs-coated CNT@PDMS straight coaxial fiber.

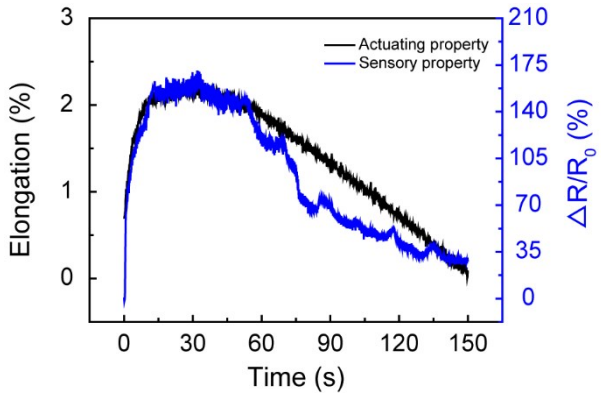

Fig. S18 Elongation and relative resistance change ($\Delta R/R_0$) as a function of time under the 2 g load.

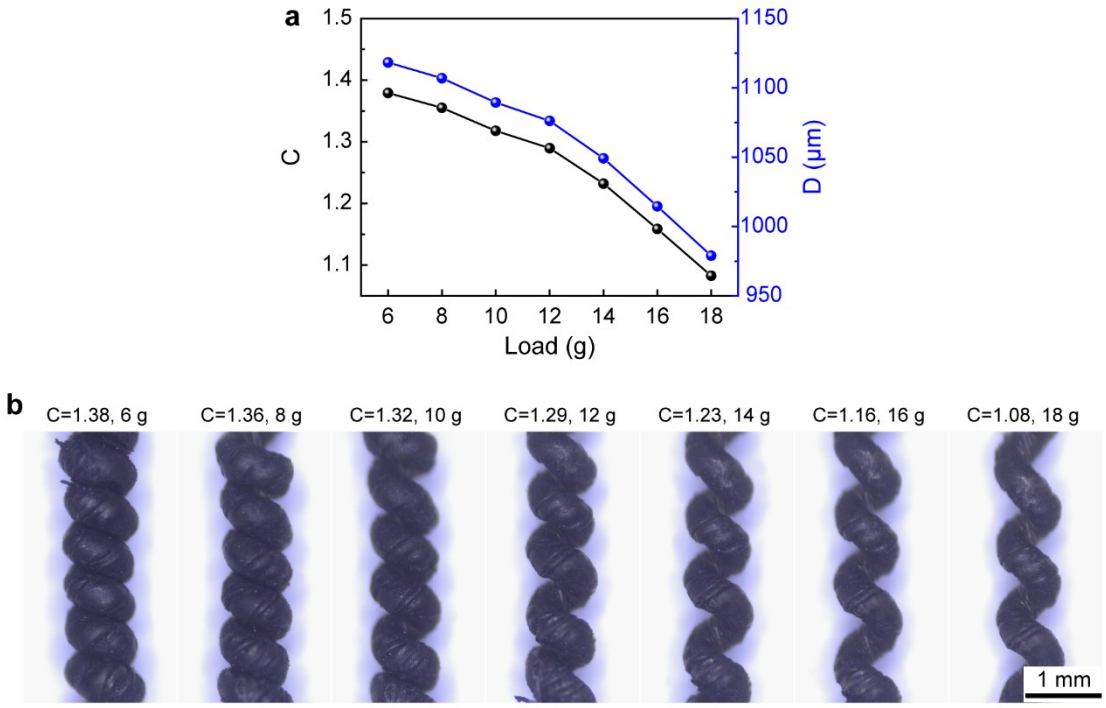

Fig. S19 (a) The spring index and the radial diameter of the MXene/SWCNTs-coated CNT@PDMS coaxial muscle fiber under different loads (6 g, 8 g, 10 g, 12 g, 14 g, 16 g and 18 g). (b) The photographs under the optical microscope of the MXene/SWCNTs-coated CNT@PDMS coaxial muscle fiber under different loads.

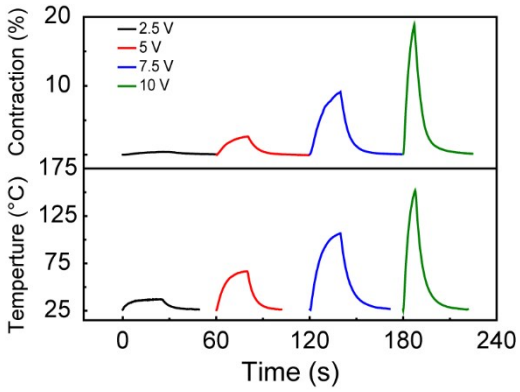

Fig. S20 Contraction and temperature as a function of time under different voltages with a 14 g load, before the coaxial muscle fiber contracts to the extreme stroke without creeping, the optimal actuating temperature of the coaxial muscle fiber under different voltages is found.

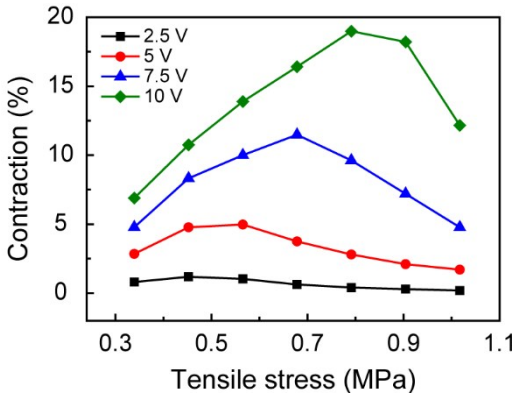

Fig. S21 The contraction of the MXene/SWCNTs-coated CNT@PDMS coaxial muscle fiber under different voltages (2.5 V, 5 V, 7.5 V and 10 V) with different loads (6 g, 8 g, 10 g, 12 g, 14 g, 16 g and 18 g).

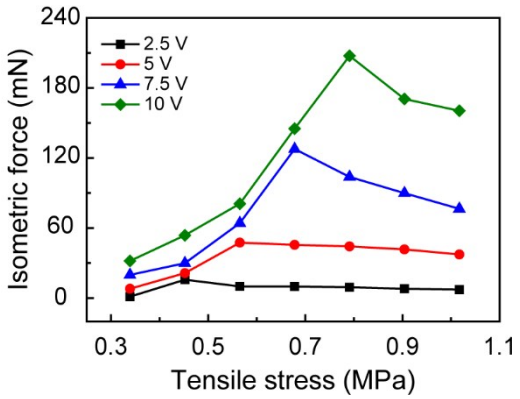

Fig. S22 The isometric stress of the MXene/SWCNTs-coated CNT@PDMS coaxial muscle fiber under different voltages (2.5 V, 5 V, 7.5 V and 10 V) with different loads (6 g, 8 g, 10 g, 12 g, 14 g, 16 g and 18 g).

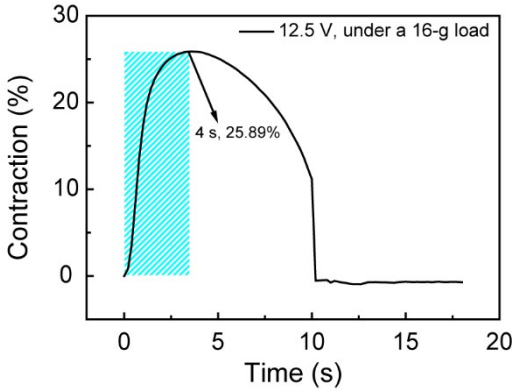

Fig. S23 The ultimate contraction after the MXene/SWCNTs-coated CNT@PDMS coaxial muscle fiber was blown by applying a 12.5 V voltage.

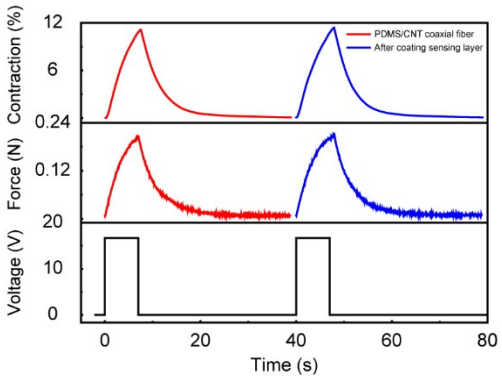

Fig. S24 The curves of the contraction and isometric force of the CNT@PDMS coaxial muscle fiber before and after coating sensing layer under a 10 V voltage with a 14 g load.

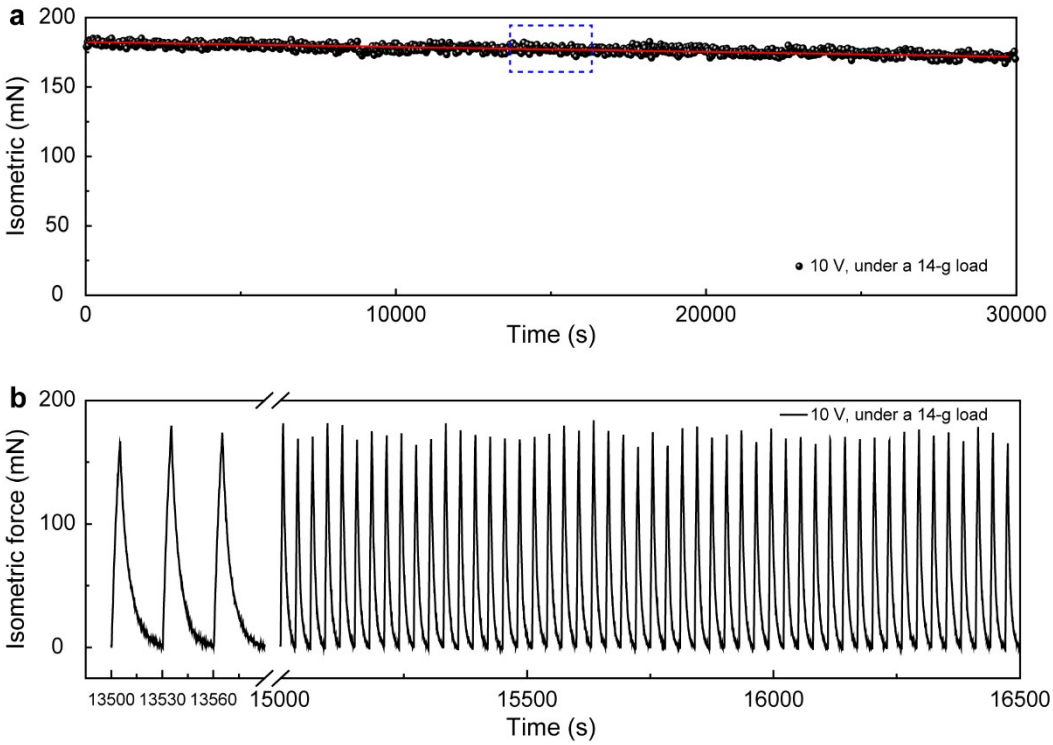

Fig. S25 (a) Cyclic tests of the isometric force (under a 10 V voltage with a 14 g load, powering on for 5 s and powering off for 25 s) on the MXene/SWCNTs-coated CNT@PDMS coaxial muscle fiber, 1 000 actuating cycles. (b) The curve of the 100 actuating cycles from 450th to 550th.

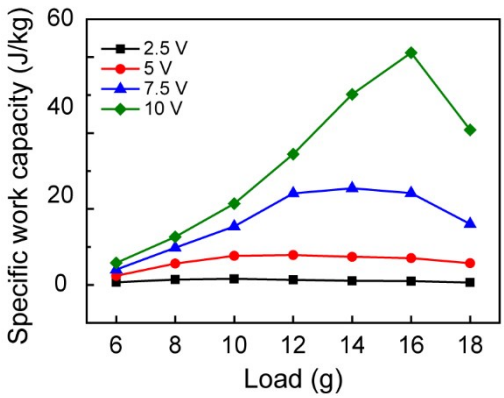

Fig. S26 The specific work capacity of the MXene/SWCNTs-coated CNT@PDMS coaxial muscle fiber under different voltages (2.5 V, 5 V, 7.5 V and 10 V) with different loads (6 g, 8 g, 10 g, 12 g, 14 g, 16 g and 18 g).

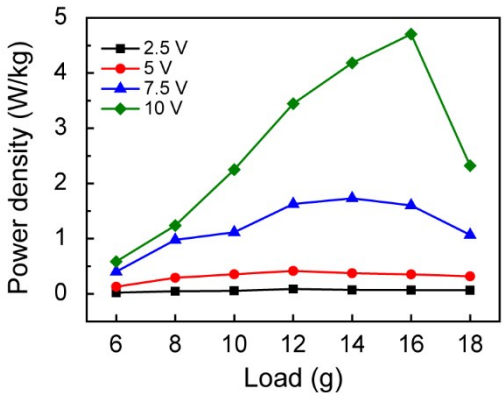

Fig. S27 The power density of the MXene/SWCNTs-coated CNT@PDMS coaxial muscle fiber under different voltages (2.5 V, 5 V, 7.5 V and 10 V) with different loads (6 g, 8 g, 10 g, 12 g, 14 g, 16 g and 18 g).

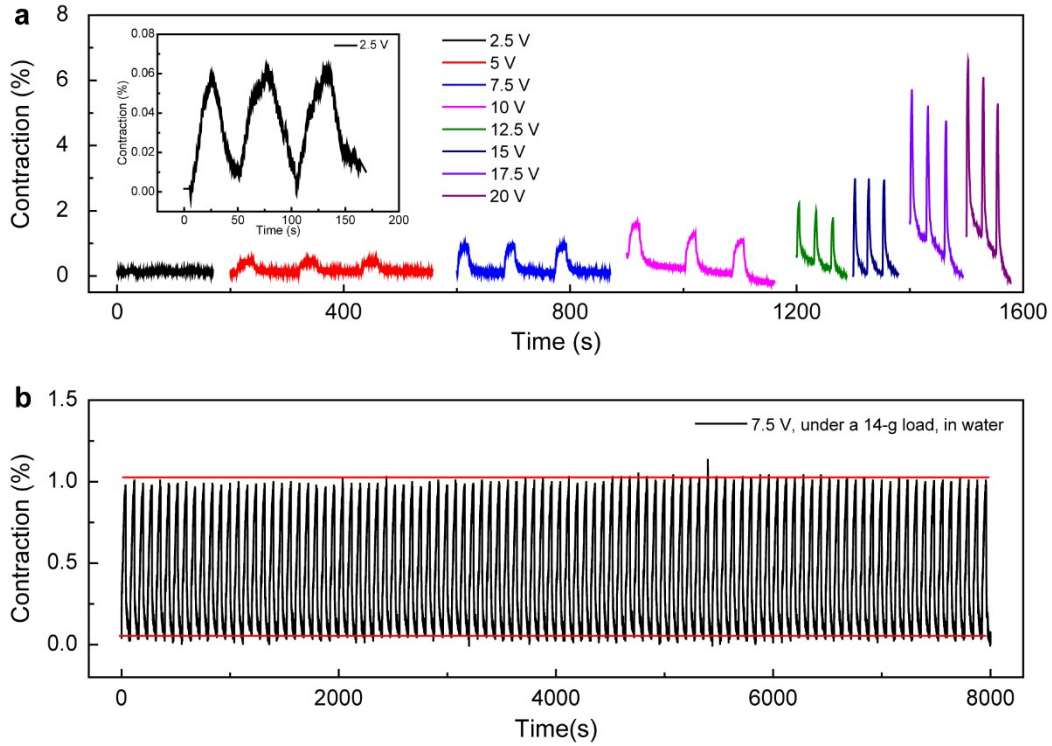

Fig. S28 (a) The contraction of the CNT@PDMS coaxial muscle fiber under different voltages (2.5 V, 5 V, 7.5 V, 10 V, 12.5 V, 15 V, 17.5 V and 20 V) with a 14 g load in water for three cycles. (b) Cyclic tests of the contraction in water (under a 7.5 V voltage with a 14 g load, powering on for 40 s and powering off for 40 s) on the PDMS/CNT coiled coaxial fiber artificial muscle 100 actuating cycles.

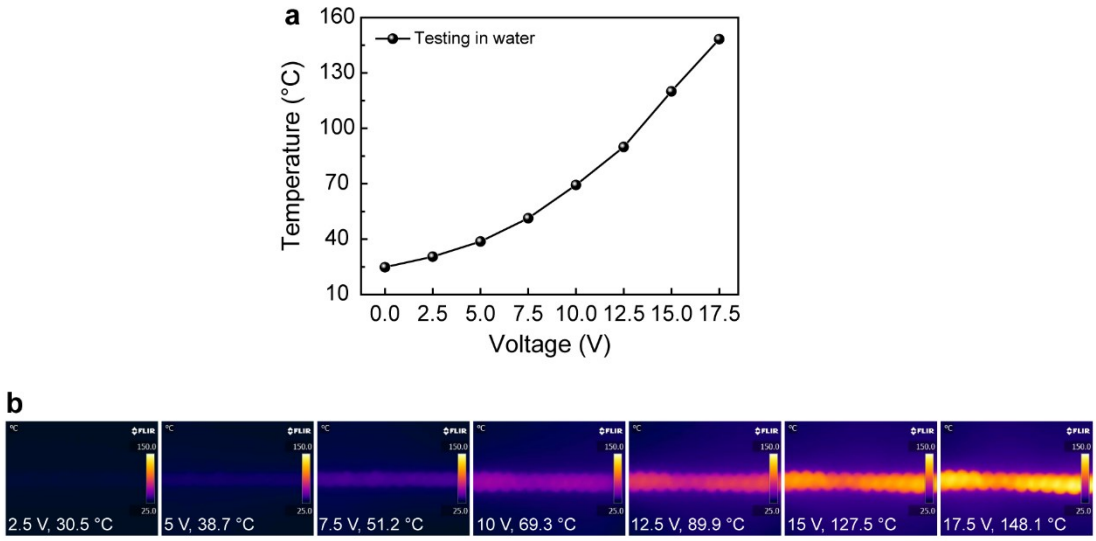

Fig. S29 (a) The temperature of the 2-cm-long CNT@PDMS coaxial muscle fiber under different voltage (2.5 V, 5 V, 7.5 V, 10 V, 12.5 V, 15 V and 17.5 V) during the contracted process in water. (b) FLIR images of the maximum actuating temperature before the end of the contracted process of the 2-cm-long CNT@PDMS coaxial muscle fiber under different voltage in water.

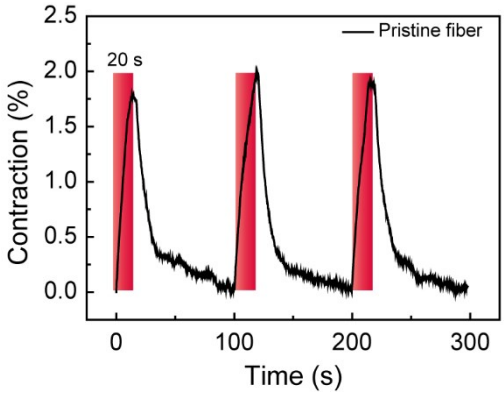

Fig. S30 The contraction of the CNT@PDMS coaxial muscle fiber driven by infrared light with a 14 g load for three cycles.

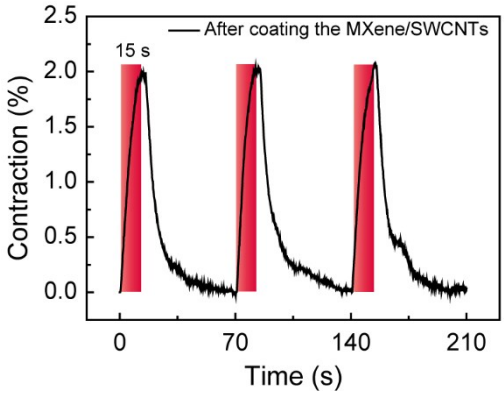

Fig. S31 The contraction of the MXene/SWCNTs-coated CNT@PDMS coaxial muscle fiber driven by infrared light with a 14 g load for three cycles.

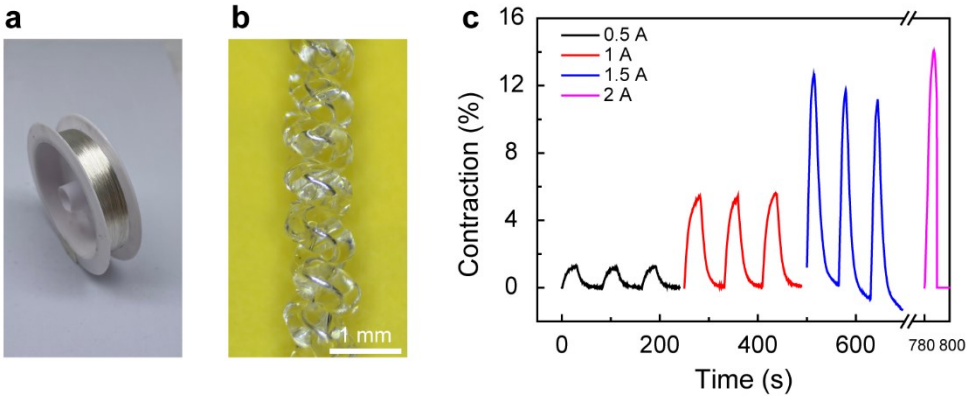

Fig. S32 (a) Photograph of a hundreds-meter-long Ag fiber winded on a mandrel. The diameter of the Ag fiber is 100 μm. (b) The photograph under the electron microscope of the Ag@PDMS coiled coaxial fiber. (c) The contraction of the Ag@PDMS coaxial muscle fiber under different currents (0.5 A, 1 A, 1.5 A and 2 A) with a 14 g load for three cycles.

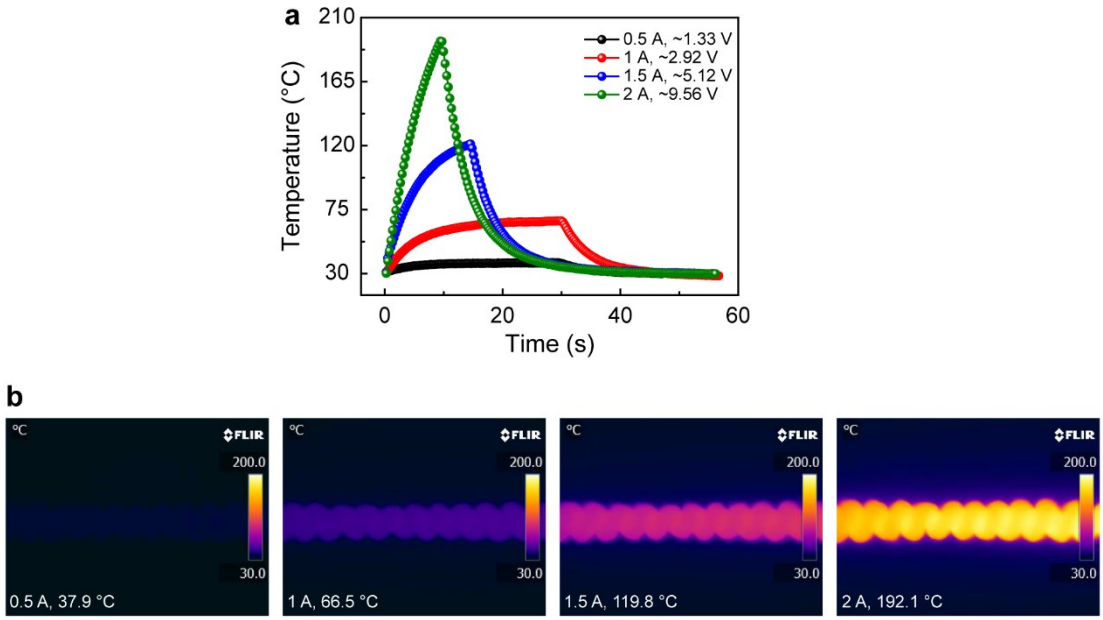

Fig. S33 (a) The temperature of the 2-cm-long Ag@PDMS coaxial muscle fiber under different currents (0.5 A, 1 A, 1.5 A and 2 A) during the contracted process. (b) FLIR images of the maximum actuating temperature before the end of the contracted process of the 2-cm-long Ag@PDMS coaxial muscle fiber under different currents.

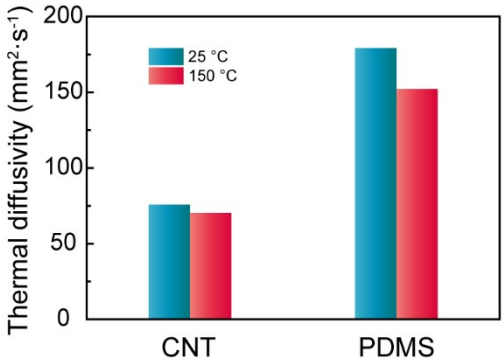

Fig. S34 The thermal diffusivity of the CNT and PDMS at 25 °C and 150 °C.

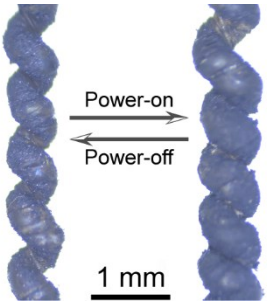

Fig. S35 The photographs under the electron microscope of electrothermally in-situ driven process of the MXene/SWCNTs-coated CNT@PDMS coaxial muscle fiber (under a 10 V voltage with a 14 g load).

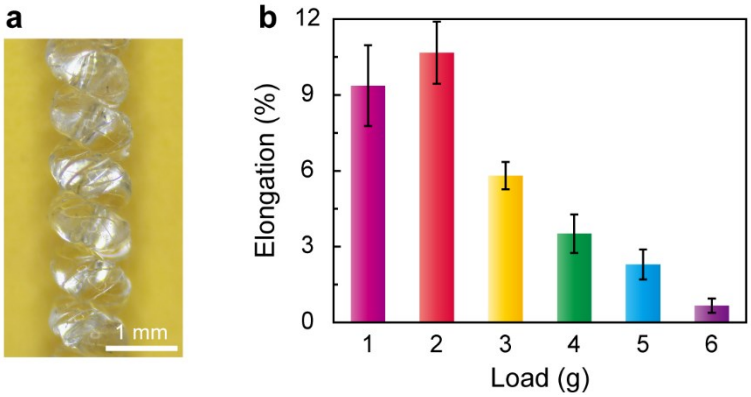

Fig. S36 (a) The photograph under the electron microscope of the PDMS muscle fiber. (b) The elongation of the PDMS muscle fiber exposed to the n-heptane solvent under different loads (1g, 2g, 3g, 4g, 5g and 6g).

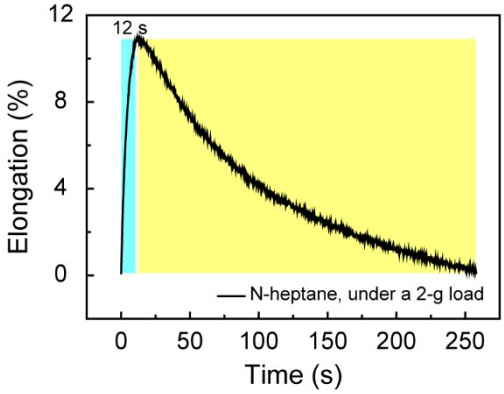

Fig. S37 The curve of the elongation as a function of time of the PDMS muscle fiber exposed to n-heptane solvent under a 2 g load.

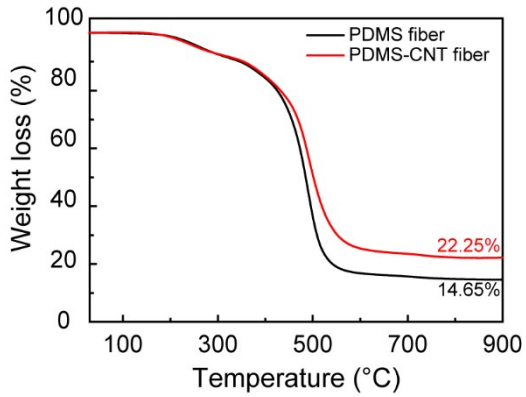

Fig. S38 The TG analysis of the CNT@PDMS fiber.

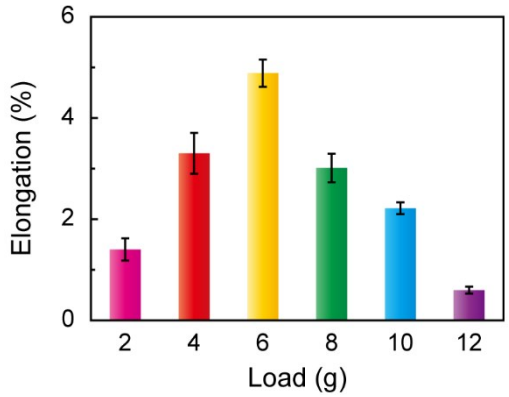

Fig. S39 The elongation of the MXene/SWCNTs-coated CNT@PDMS coaxial muscle fiber exposed to n-heptane solvent under different loads.

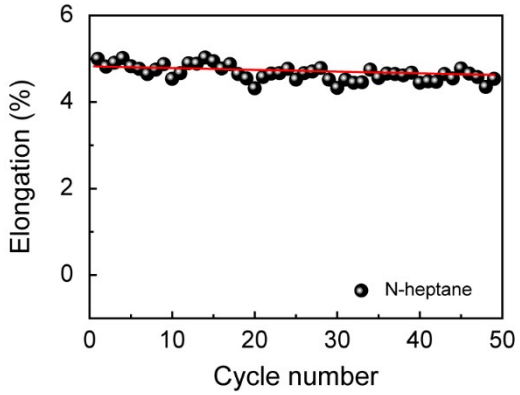

Fig. S40 Cyclic tests (exposed to n-heptane solvent under a 6 g load) on the MXene/SWCNTs-coated CNT@PDMS coaxial muscle fiber, 50 actuating cycles.

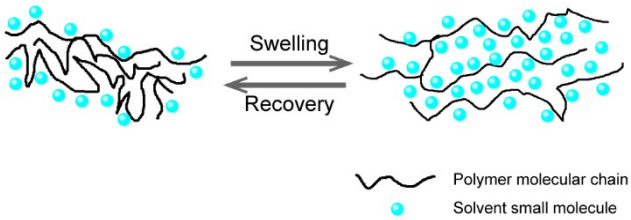

Fig. S41 Swelling process of amorphous polymers and solvents with similar polarities.

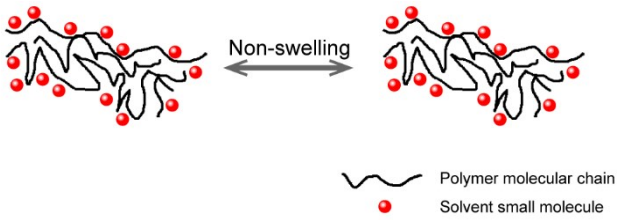

Fig. S42 Solvent small molecules and polymer molecular chain with the different polarities are immiscible.

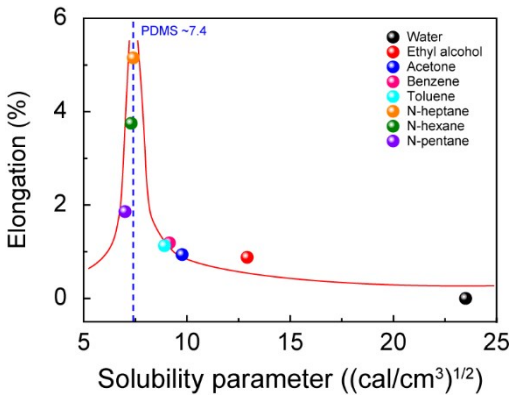

Fig. S43 The relationship between solubility parameters of different solvents and the elongation of the CNT@PDMS coaxial muscle fiber.

Fig. S44 The bundling of 20-ply CNT@PDMS coaxial muscle fiber.

Table S1. Comparison of the tensile contraction and the work capacity between the literature results for electrothermal coiled muscle fibers composed of CNT/polymer and the present results for our CNT@PDMS coaxial muscle fiber.

Materials	Contraction (%)	Work capacity (J kg^{-1})	Ref.
Typical mammalian skeletal muscles	~20	7.7	[1]
CNT and silicone rubber	~7	-	[2]
CNT and paraffin waxes	7.3	160	[3]
CNT and polyethylene oxide (PEO-SO_3)	~8	1050	[4]
CNT and silicone elastomers	9.7	490	[5]
CNT and epoxy resin	12	-	[6]
CNT and polyurethane (PU)	~13	1100	[4]
CNT and thermoplastic polyurethanes (TPU)	~13.8	78.6	[7]
CNT and PDMS	19	61.2	**This work**

Table S2. The dielectric constant, polarity, and solubility parameter of different solvents; the elongation of the CNT/PDMS coaxial muscle fiber in response to different solvents.

Solvent	Permittivity $C^2/(N \cdot M^2)$ [8]	Polarity	Solubility parameter $(cal/cm^3)^{1/2}$ [8]	Elongation %
Water	78.5 (25 °C)	Polar	23.50	0
Ethyl alcohol	24.3 (25 °C)		12.92	0.88
Acetone	20.7 (25 °C)		9.77	0.94
Benzene	2.27 (25 °C)	Non-polar	9.15	1.19
Toluene	2.38 (25 °C)		8.91	1.13
PDMS	2.75 (25 °C)		~7.4	-
N-heptane	1.8 (20 °C)		7.4	5.15
N-hexane	1.9 (25 °C)		7.3	3.75
N-pentane	1.8 (20 °C)		7.0	1.86

References:

1 T. Mirfakhrai, J. D. W. Madden and R. H. Baughman, *Mater. Today*, 2007, **10**, 30-38.

2 M. D. Lima, M. W. Hussain, G. M. Spinks, S. Naficy, D. Hagenasr, J. S. Bykova, D. Tolly and R. H. Baughman, *Small*, 2015, **11**, 3113-3118.

3 M. D. Lima, N. Li, M. Jung de Andrade, S. Fang, J. Oh, G. M. Spinks, M. E. Kozlov, C. S. Haines, D. Suh, J. Foroughi, S. J. Kim, Y. Chen, T. Ware, M. K. Shin, L. D. Machado, A. F. Fonseca, J. D. Madden, W. E. Voit, D. S. Galvao and R. H. Baughman, *Science*, 2012, **338**, 928-932.

4 J. Mu, M. Jung de Andrade, S. Fang, X. Wang, E. Gao, N. Li, S. H. Kim, H. Wang, C. Hou, Q. Zhang, M. Zhu, D. Qian, H. Lu, D. Kongahage, S. Talebian, J. Foroughi, G. Spinks, H. Kim, T. H. Ware, H. J. Sim, D. Y. Lee, Y. Jang, S. J. Kim and R. H. Baughman, *Science*, 2019, **365**, 150-155.

5 S. P. Dai, X. S. Zhou, X. H. Hu, X. Dong, Y. Y. Jiang, G. G. Cheng, N. Y. Yuan and J. N. Ding, *Acs Applied Nano Materials*, 2021, **4**, 5123-5130.

6 L. Xu, Q. Peng, Y. Zhu, X. Zhao, M. Yang, S. Wang, F. Xue, Y. Yuan, Z. Lin, F. Xu, X. Sun, J. Li, W. Yin, Y. Li and X. He, *Nanoscale*, 2019, **11**, 8124-8132.

7 Y. Song, S. Zhou, K. Jin, J. Qiao, D. Li, C. Xu, D. Hu, J. Di, M. Li, Z. Zhang and Q. Li, *Nanoscale*, 2018, **10**, 4077-4084.

8 M. Rubinstein, R. H. Colby, *Polymer Physics (Chemistry)*, 2011, **9**, 019852059X.